
Article:
Balikhin, M.A., Runov, A., Walker, S.N. orcid.org/0000-0002-4105-1547 et al. (4 more authors) (2014) On the fine structure of dipolarization fronts. Journal of Geophysical Research: Space Physics, 119 (8). pp. 6367-6385. ISSN 2169-9402

https://doi.org/10.1002/2014JA019908

AGU PUBLICATIONS

JGR

Journal of Geophysical Research: Space Physics

RESEARCH ARTICLE

10.1002/2014JA019908

Key Points:
- The fine structure of the dipolarization front is described
- Identification of oscillations within the dipolarization front are presented
- The bipolar structure of the electric field within dipolarization front is shown

Correspondence to:
M. A. Balikhin,
m.balikhin@sheffield.ac.uk

Citation:
Balikhin, M. A., A. Runov, S. N. Walker, M. Gedalin, I. Dandouras, Y. Hobara, and A. Fazakerley (2014), On the fine structure of dipolarization fronts, *J. Geophys. Res. Space Physics*, *119*, 6367–6385, doi:10.1002/2014JA019908.

Received 21 FEB 2014
Accepted 24 JUL 2014
Accepted article online 28 JUL 2014
Published online 22 AUG 2014

On the fine structure of dipolarization fronts

M. A. Balikhin[1], A. Runov[2], S. N. Walker[1], M. Gedalin[3], I. Dandouras[4,5], Y. Hobara[6], and A. Fazakerley[7]

[1]Department of Automatic Control and Systems Engineering, University of Sheffield, Sheffield, UK, [2]Institute of Geophysics and Planetary Physics, University of California, Los Angeles, California, USA, [3]Department of Physics, Ben-Gurion University, Beer-Sheva, Israel, [4]UPS-OMP, IRAP, Toulouse, France, [5]CNRS, IRAP, Toulouse, France, [6]Department of Communication Engineering and Informatics, University of Electro-Communications, Chofu, Japan, [7]Mullard Space Science Laboratory, University College London, London, UK

Abstract Measurements from the closely spaced Cluster spacecraft are used to study the structure of the magnetic and electric fields within the magnetic ramp of dipolarization fronts (DF) observed close to the neutral sheet and the midnight meridian ($Y_{GSM} < 3\,R_E$). The spacecraft separation was small enough (<300 km) to treat the magnetic ramp of the DF front as a planar structure as indicated from variance analysis. The finite value of the magnetic field along the minimum variance direction for the events studied indicates that the dipolarization front structure was distinct from a tangential discontinuity. In addition to the main increase of the magnetic field in the maximum variance component, strong oscillations were observed in the intermediate component. The presence of this oscillatory structure results in an expansion of the region in which a change of magnetic pressure occurs, the size of which is typically an ion Larmor radius or greater. This widening is important in maintaining the pressure balance at the edge of the DF. This phenomenon resembles observations of intense current sheets in the magnetotail and also laboratory experiments of current sheet formation, in which a similar widening of the ramp region has been observed. In this paper we argue against the idea that an electron temperature anisotropy, resulting in electron curvature currents, can explain the formation of the oscillatory structures observed at DFs. These oscillations can be explained as eigenmode waves of the plasma that propagate away from the disturbance (DF) that is moving at subsonic speeds. Oscillations observed within the magnetic ramp indicate field-aligned currents that are expected to be associated with DF.

1. Introduction

A sudden, rapid, high-amplitude increase in the northward magnetic field component (B_z), which is typically observed at the leading edge of fast plasma flows in the near-Earth magnetotial, is often referred to as a dipolarization front (DF) [e.g., *Nakamura et al.*, 2002b; *Runov et al.*, 2009]. The fronts have been observed at a variety of geocentric distances from −30 to −5 R_E [*Ohtani et al.*, 2004]. Analysis of multipoint observations has shown that the fronts are thin boundaries with a thickness comparable to an ion thermal gyroradius separating the energetic and tenuous plasma of fast flows (plasma jet) from the ambient plasma sheet [*Runov et al.*, 2011]. The plasma jets, forming bursty bulk flows [*Angelopoulos et al.*, 1992], are widely recognized to be magnetotail reconnection outflows. Thus, the DFs originate during pulses of magnetotail reconnection [*Sitnov et al.*, 2009; *Runov et al.*, 2012; *Angelopoulos et al.*, 2013]. It has been shown, however, that front-like structures may appear due to the interchange or ballooning instability [*Pritchett and Coroniti*, 2010, 2011]. The two scenarios, reconnection and interchange, are not necessarily mutually exclusive: the edge of reconnection jet was shown to be interchange unstable [e.g., *Nakamura et al.*, 2002a].

Although dipolarization front structure has been a subject of many recent studies, including statistical analyses of large data sets [e.g., *Schmid et al.*, 2011; *Fu et al.*, 2011; *Liu et al.*, 2013], the fine structure of the DF still needs to be investigated. One of the problems is that the DF is a thin boundary (a current sheet) that passes over the satellite in a very short time (1 to a few seconds). To resolve its structure, multipoint measurements with a probe separation smaller than the front thickness are needed. During the 2003 tail season the Cluster constellation had the separation of less than 300 km. This separation is smaller than the typical thickness of the DF (~500 to 1000 km [see *Runov et al.*, 2011]). Event studies of DF observations by Cluster with the separation of ~200 km may shed a light on the internal structure of fronts, which are often considered as tangential discontinuities [e.g., *Sergeev et al.*, 2009; *Khotyaintsev et al.*, 2011]. While on large scales compared to the thermal ion gyroradius DFs may indeed be described as tangential discontinuities, on small,

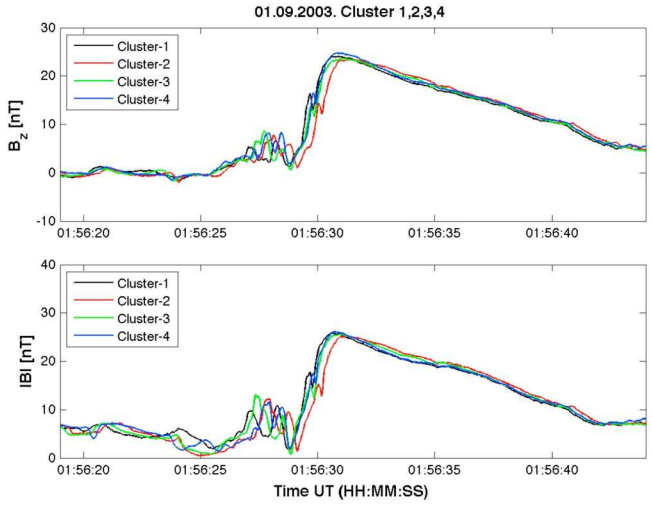

Figure 1. B_Z (GSM) component of (top) the magnetic field and (bottom) the magnetic field magnitude as measured by the four Cluster spacecraft during the observation of DF on 1 September 2003.

subgyroscales DFs are complex and structured current sheets that may embed small-scale dissipative layers [*Angelopoulos et al.*, 2013].

Magnetic field oscillations are often observed ahead of the front, on its ramp, and behind the front. These have been interpreted as whistler modes [*Khotyaintsev et al.*, 2011], lower hybrid drift waves, and signatures of the interchange instability at the front [e.g., *Pritchett and Coroniti*, 2010, 2011; *Vapirev et al.*, 2013]. Studies of the magnetic and electric field oscillations at the front based on multipoint measurements using closely separated probes provide an opportunity to distinguish between spatial structures and temporal variations and accurately estimate their phase velocity and wavelength.

In this paper we present detailed observations of DFs observed during July–October 2003 when the separation between Cluster spacecraft was small enough to resolve the fine structure of the fronts. We have studied the internal structure of the front and magnetic oscillation ahead of the DF ramp.

2. Data and Instrumentation

The data sets used in this study were collected by the Cluster II satellites during the period July–October 2003 when the interspacecraft separation in the magnetotail was small, typically less than 300 km. The motivation for using these periods was to avoid the effects of nonplanarity of the structure. The magnetic and electric field measurements were made by the fluxgate magnetometer FGM [*Balogh et al.*, 1997] and Electric Fields and Waves (EFW) instruments [*Gustafsson et al.*, 1997], respectively. EFW is a part of Cluster Wave Consortium (WEC) [*Pedersen et al.*, 1997], a suite of plasma wave instruments centrally controlled by the Digital Wave Processor (DWP) instrument [*Woolliscroft et al.*, 1997]. The EFW instrument consists of two pairs of spherical probe sensors, each on a 44 m wire boom in the spin plane of the satellite. Ion data are taken from the COmposition and DIstribution Function analyser (CODIF) sensor of the Cluster Ion Spectrometry (CIS) instrument [*Rème et al.*, 2001]. In the following sections the structure of two DF events, observed on 1 and 12 September 2003, are discussed in detail together with possible mechanisms for their occurrence.

3. DF Event: 1 September 2003 at 1:56 UT

Figure 1 displays the Z component (top) and modulus (bottom) of the magnetic field as measured by the four Cluster spacecraft during time period 01:56:19–01:56:44 UT on 1 September 2003. During this observation Cluster 1 was located at a position [−118287, −10395, 220] km GSM and traveling earthward. The spacecraft separation vectors for pairs 1-2, 1-3, and 1-4 are (−45, −215, 92), (105, −194, 64), and (19, −28, 209) km GSM, respectively, and their relative positions (in the GSE frame) are shown in Figure 2. The closeness of the satellites to the neutral sheet is evident not only from the value of the Z coordinate of spacecraft during the observations but also from the value of B_X (< 1 nT) in the time interval just preceding the DF (not shown). During this period all four spacecraft observe the passage of a DF at around 01:56:29 UT, as indicated by the sharp increase or ramp-like feature in the B_Z component of the magnetic field. The duration of this main ramp is about a second in which time the B_Z component increases from around zero before the DF to a maximum value of 24 nT. At the beginning of the interval shown in Figure 1 the absolute value of the magnetic field is about 5 nT. Around 01:56:25 UT, $|B|$ decreases. This is especially evident in the field profiles from Cluster 2 and Cluster 4. For these two spacecraft $|B|$ drops as low as 1 nT. Such a small value of $|B|$ implies a low value of B_X, indicating close proximity to the neutral sheet. After reaching its maximum,

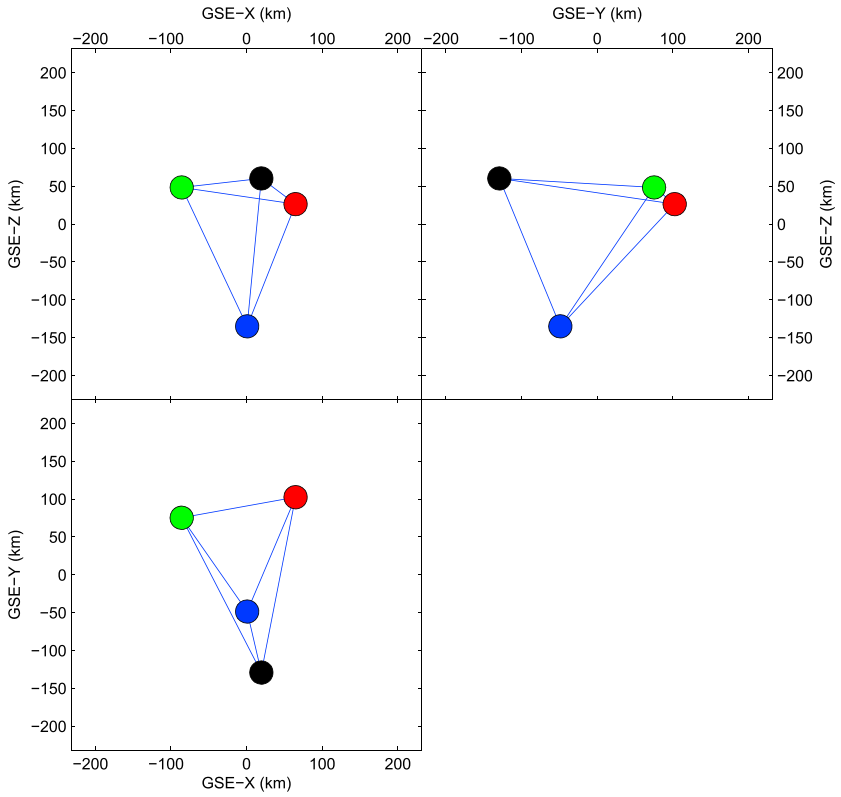

Figure 2. The configuration of the Cluster satellites on 1 September 2003 at 01:56:00.

the B_Z component decreases monotonically over a period that lasts approximately 10 s as the magnetic field relaxes back to its pre-DF level. Qualitatively, the evolution of the magnetic field magnitude is similar to that of the B_Z component. A peculiar feature of the main ramp, observed by all spacecraft in both B_Z and $|B|$, is that they are not monotonic but exhibit a local maxima in the center of the main transition. Similar features have also been observed for a large portion (11 out of 15 (73%)) of the DF investigated during the selection of the six events presented in this paper. The similarity of the magnetic profiles shown in Figure 1 also illustrates that the Cluster spacecraft are close enough to separate temporal and spatial variations.

3.1. Normal and Velocity of the DF

The four Cluster spacecraft are in sufficiently close proximity to one another to assume planarity of the magnetic ramp structure on corresponding spatial scales. This assumption can be validated by the analysis of the local normals at each observation point. For any magnetic structure, the local normals will be parallel to the minimum variance direction ($\mathrm{div}\,\mathbf{B} = 0$). The spread of the minimum variance directions identified using the data from each spacecraft data can be used to assess the planarity of the observed DF on scales corresponding to the spacecraft separations. Data from the entire extent of the magnetic ramp region, as observed by each individual spacecraft, were subjected to a variance analysis. The time intervals that were used for Minimum Variance Analysis (MVA) were 01:56:29.00–01:56:30.61, 01:56:28.82–01:56:30.96, 01:56:28.86–01:56:30.55, and 01:56:28.55–01:56:30.69 UT for Cluster 1, Cluster 2, Cluster 3, and Cluster 4, respectively. The minimum variance directions identified were well defined for all four spacecraft. The ratios of the intermediate to minimum eigenvalues were in the range 34–150. The range for the ratios of the maximum to intermediate eigenvalues was 4.8–10. The resulting minimum variance directions were very closely aligned to each other, separated by angles in the range 1°–7°. The minimum variance direction, averaged over the four spacecraft, was $n_a = [0.83, 0.48, -0.28]$ (GSM). The spread of angles between the various pairs of maximum variance directions lies in the range 1°–5°. The close alignment of the individual minimum and maximum variance directions allows us to treat the surface of the B_Z ramp as a planar structure on spatial scales or the order of the satellite separation distances. Assuming that the motion of the leading edge of the DF structure is along its normal direction n_a, the time delay between spacecraft can be used to

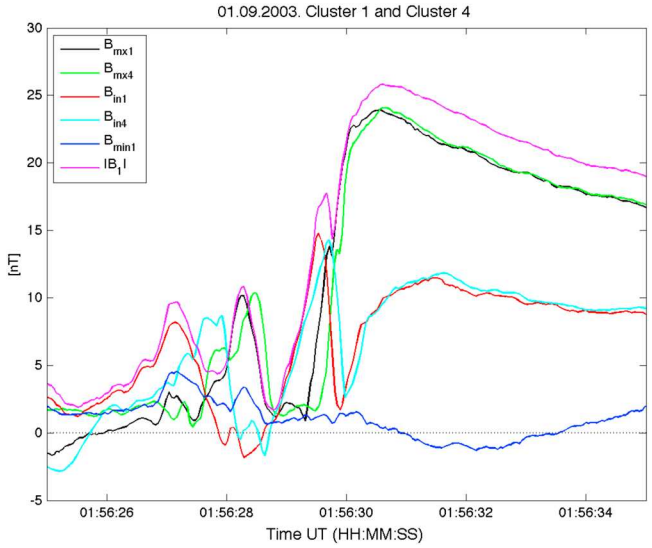

Figure 3. Modulus (magenta) of the magnetic fields as measured by Cluster 1 and components of the magnetic field on the maximum (Cluster 1, black; Cluster 4, green), intermediate (Cluster 1, red; Cluster 4, cyan), and minimum (Cluster 1, blue) variance directions identified from Cluster 1 data during the observation of DF on 1 September 2003.

identify its velocity. It can be seen that the local maximum around the center of $|B|$ and B_Z is observed by all spacecraft. For spacecraft 1 and 4 this maximum of $|B| \sim 17.7$ nT and is observed fairly centrally within the ramp region. In contrast, the local maxima observed by spacecraft 2 and 3 are slightly lower (15.2 and 14.6 nT, respectively) and appear to be shifted toward the lower end of the ramp. This similarity between spacecraft pairs 1-4 and 2-3 and the difference in the observation of this local maximum together with spacecraft separation vectors indicates that its position within the ramp depends upon the Y coordinate of the satellite location. For a reliable determination of the DF velocity the pairs 1-4 and 2-3 were used because of the similarity in the ramp profiles. The separation of spacecraft 1 and 4 along the averaged normal n_a was 57 km. The modulus (magenta) and three components of the magnetic field as measured by Cluster 1 along the maximum (B_{max1}, black), intermediate (B_{int1}, red), and minimum (B_{min1}, blue) variance directions are plotted in Figure 3. The projections of the magnetic field, as measured by Cluster 4 along the same maximum and intermediate variance directions, are also shown in Figure 3 by the green (B_{max4}) and cyan (B_{int4}) curves. The close similarity between the profiles of the B_{max} and B_{int} components measured by these two spacecraft enables an accurate determination of the time delay between them. This time delay (0.126 s) implies that the velocity of the structure along the normal direction was 453 ± 70 km/s. Analysis of the evolution of the variance frame components B_{max} and B_{int} components measured by Cluster 2 and 3 were also very similar in nature, with a time delay of 0.316 s between the signals. The separation between the spacecraft 2 and 3 along the normal n_a was 143 km, resulting in a velocity estimate of 452 ± 35 km/s. Such close similarity between the values of velocity identified by pairs 1-4 and 2-3 was not expected but provides confidence in the accuracy of the velocity estimate.

It is evident from Figure 3 that B_{min1} has a finite, nonzero value during the ramp crossing. The minimum variance component for Cluster 4 spacecraft (not shown) is also nonzero. This finite value of the normal magnetic field component for this event is in contradiction with the assumption of *Fu et al.* [2012] that the leading edge of a DF can be treated as a tangential discontinuity. Strictly speaking, MHD terminology is not directly applicable to a structure that may be described by kinetic processes, such as a DF. There are no physical arguments to suggest that a DF necessarily represents one of the discontinuities that exist in MHD: contact, tangential, rotational, or MHD shock. It could, for instance, be a nonlinear structure that differs from all four. *Fu et al.* [2012] tried to show that there is no flow of plasma across the DF and used the results obtained to state that a DF is a tangential discontinuity, while the only conclusion that can be drawn from such a study (providing it is correct!) is that the DF is a nonlinear structure with no plasma flow across it. Therefore, it is worth investigating the reliability of the nonvanishing normal component (B_{min1}) in Figure 3. To estimate statistical errors in the value of the B_{min1}, a methodology was developed by Sonnerup and coworkers and summarized in *Sonnerup and Scheible* [1998]. According to equation (8.24) of *Sonnerup and Scheible* [1998] the composite statistical error estimate for B_{min} ($\langle \delta B_{\mathrm{min}} \rangle$) is

$$\langle \delta B_{\mathrm{min}} \rangle = \sqrt{\frac{\lambda_{\mathrm{min}}}{N-1} + \left(\Delta\phi_{32}\langle \mathbf{B} \rangle \cdot \mathbf{e_2}\right)^2 + \left(\Delta\phi_{31}\langle \mathbf{B} \rangle \cdot \mathbf{e_1}\right)^2}, \quad (1)$$

where λ_{min} is the minimum variance eigennumber, N number of data points used for MVA, $\langle \mathbf{B} \rangle$ averaged vector of the magnetic field, and $\mathbf{e_1}, \mathbf{e_2}$ are the unit vectors in the maximum and intermediate variance

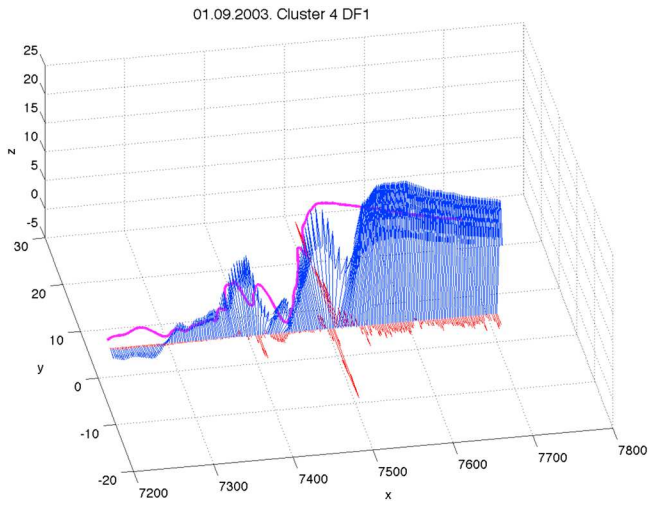

Figure 4. $|B|$ (magenta), spatial evolution of the magnetic field vector in GSM coordinates, and the E_X (red) as measured by Cluster 4 through the DF on 1 September 2003. Magnetic field data are resampled to electric field measurement times. The electric field data point number since the beginning of the interval under investigation are shown for the *x* axis.

directions. The values $\Delta\phi_{3i}$ are the angular error estimates in radians [see *Sonnerup and Scheible*, 1998, equation (8.23)]:

$$\phi_{3i} = \sqrt{\frac{\lambda_{\min}}{N-1}\frac{\lambda_i}{(\lambda_i - \lambda_{\min})^2}}, i = 1, 2, \quad (2)$$

where λ_1, λ_2 are the maximum and intermediate variance eigenvalues, respectively. The parameters resulting from MVA for data from Cluster 1 are as follows: $N = 41$, $\lambda_{\min} = 0.0931$, $\lambda_1 = 85.5778$, and $\lambda_2 = 14.3329$. To determine an upper limit for the error, we replace $\langle \mathbf{B} \rangle \cdot \mathbf{e_2}$ and $\langle \mathbf{B} \rangle \cdot \mathbf{e_1}$ by the maximum value of $B_{\max}$ from Figure 3, namely, 25 nT. The resulting value of $\langle \delta B_{\min} \rangle$ is about 0.35 nT. It can be seen that value of $B_{\min}$ within the ramp is about 2–3 times greater than the composite statistical error estimate $\langle \delta B_{\min} \rangle$. It must be noted that 0.35 nT represents an upper bound for $\langle \delta B_{\min} \rangle$. A more accurate calculation of this error using equation (1) without replacing $\langle \mathbf{B} \rangle \cdot \mathbf{e_2}$ and $\langle \mathbf{B} \rangle \cdot \mathbf{e_1}$ by the maximum value of $B_{\max}$ will lead to the even lower value of $\langle \delta B_{\min} \rangle$.

A peculiar feature seen in Figure 3 is the simultaneous observation by both spacecraft of oscillations in the B_{int} component at the same time as the increase in the $B_{\max}$ component. For example, at 01:56:28.9 UT the B_{int} component begins to increase from a value of about 1 nT and reaches a maximum of 14.5 nT at 01:56:29.5 UT before decreasing to a minimum of ≈1.6 nT at 01:56:29.9 UT. After this minimum B_{int} again increases up to a value 8 nT at 01:56:30.3 UT. The period of these oscillations (1–2 s) is too large to be attributed to either the lower hybrid drift (~5–15 Hz) or whistler waves (~100 Hz) that are usually observed in the vicinity of a DF [*Khotyaintsev et al.*, 2011]. Another illustration of these oscillations is shown in Figure 4 in which a 3-D view of the evolution of the magnetic field through the DF is presented. The *X* axis represents the point number of the magnetic field data which results in a more convenient scale for comparison with the *Y* and *Z* axes. Figures 3 and 4 clarify the origin of the nonmonotonic increase of the B_Z and $|B|$ and the local maximum observed within their ramps. As can be seen from Figure 3 just prior to the beginning of and during the initial part of the $B_{\max}$ ramp, the dominant component of the magnetic field is B_{int}. At this time the modulus of the magnetic field almost coincides with the value of B_{int}. Once B_{int} reaches its maximum and begins to decrease, the relative contribution of $B_{\max}$ to the modulus becomes the dominant component. However, the field within transition region between B_{int} and $B_{\max}$ dominance of $|B|$ does not vary monotonically. It is observed that the B_{int} component begins to decrease before $B_{\max}$ becomes the dominant component. Since the *Z* GSM direction does not coincide exactly with the maximum variance direction, the B_Z components shown in Figure 1 contain contributions from both $B_{\max}$ and B_{int}. This explains the similar nonmonotonic ramp profiles of the B_Z components that are observed by all four spacecraft in Figure 1. It should be noted that the nonmonotonic feature seen in the $B_{\max}$ ramp was also observed by spacecraft 1 and 4 data (as shown in Figure 3). However, this feature is much less prominent than that which was observed in the $|B|$ component in the same figure or the B_z curve shown in Figure 1 (top). This can be explained by the finite accuracy achieved in the determination of maximum variance direction for these satellites.

It can be seen from Figure 4 that the oscillation in B_{int} observed during the magnetic ramp is part of a set of similar oscillations that are observed earthward, i.e., before the DF. Their magnitude decreases with distance upstream of the DF. To some extent they are reminiscent of a whistler wave precursor observed upstream of a subcritical, collisionless shock. However, elliptically polarized whistlers lead to a rotation of the magnetic field upstream of the shock. Such a rotation is absent in Figure 4. Instead, the change of the magnetic field

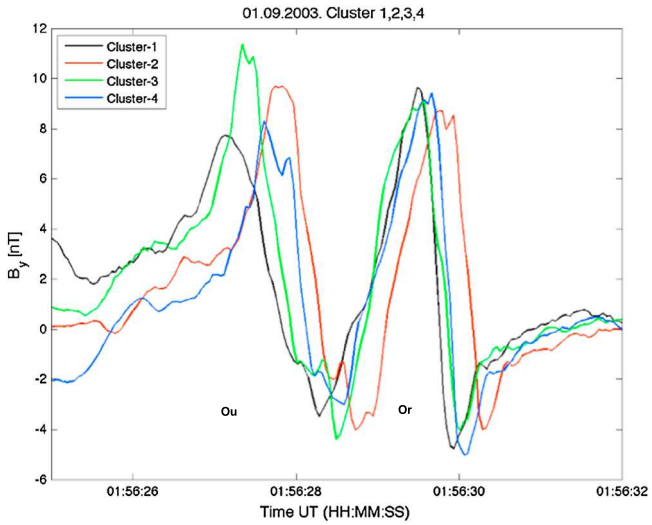

Figure 5. B_Y (GSM) component as observed by all four Cluster spacecraft during the time interval 01:56:25–01:56:32 UT on 1 September 2003. The two oscillations O_u and O_r are highlighted.

direction occurs mainly due to the variation of the component of the magnetic field that is close to B_Y. Figure 5 displays variations of B_Y (GSM) component as observed by all four Cluster spacecraft during time interval 01:56:25–01:56:32 UT. The presence of at least two oscillations in B_Y, the first centered around 01:56:27–28 and a second at 01:56:29–30, is evident in this figure. The latter oscillation is observed during the crossing of the main $|B|$ ramp and was discussed above. In the following sections of this report, this oscillation will be referred to as O_r (oscillation at the ramp). The other oscillation in B_Y that was observed about 2 s earlier will be referred to as O_u (oscillation upstream). It can be seen that all four Cluster spacecraft observed very similar profiles of the magnetic field for O_r. This is in agreement with the similarity of the maximum, intermediate, and minimum variance directions for all four spacecraft as discussed above. In contrast, the profiles of B_Y measured by the different spacecraft for O_u exhibit significant differences. It is also obvious from Figure 5 that if the wavefront related to O_u can be treated as a planar structure, its normal will deviate from that of O_r since the time shift between spacecraft 2 and 4 in the observation of O_r is about 0.3 s, while O_u is observed almost simultaneously by this pair of spacecraft. Therefore, the separation direction between Cluster 2 and Cluster 4 should be very close to the plane of wavefront for O_u and deviate significantly from the wavefront of O_r. The maximum, intermediate, and minimum variance directions for O_u identified for all four Cluster spacecraft display significant differences. The angular differences between the minimum variance directions determined for each spacecraft lie in the range from 8° (Cluster 2 and Cluster 4) to 29.7° (Cluster 1 and Cluster 3). The minimum variance direction for Cluster 3 exhibits the largest deviations with respect to those of the other spacecraft (C1 29.7°, C2 17.8°, and C4 25.4°). If the results from spacecraft 3 are neglected, the angular range between the normals lie in the range 8° to 17.8° (pair 1-2). The separation direction between spacecraft 2 and 4 and their minimum variance directions differ by angles of 80.8° and 85.4°, respectively; i.e., the spacecraft is almost perpendicular to the direction of propagation of O_u. This is in accordance with the almost simultaneous observation of O_u by Cluster 2 and 4 that is evident from Figure 5, resulting in large errors for the determination of the velocity of O_u using the time delay between these two spacecraft. As a result, only two pairs of satellites, namely, 1-2 and 1-4, have been used to estimate the velocity of O_u. The angle between the separation vector between Cluster 1 and Cluster 2 and the average of their minimum variance directions $ka_{12} = [-0.61, -0.21, 0.77]$ is 53°. This acute angle should enable a reasonable estimate of the O_u velocity to be made. The time delay in the observation of O_u between these two spacecraft is about 0.58 s resulting in an estimate for the velocity as 245 km/s. For the pair 1-4 the angle between the separation and the average minimum variance direction $ka_{14} = [-0.55, -0.21, 0.81]$ is 39° and the corresponding time delay is 0.53 s, resulting in a velocity of 310 km/s. Both estimates (310 km/s and 245 km/s) should be treated as very approximate because of the significant difference in the profiles of O_u as observed by Cluster 1, Cluster 2, and Cluster 4. A second method to estimate the velocity and wavefront normal of O_u can be made using the time difference between the observations by all four spacecraft together with their relative positions to the estimate of the velocity and orientation of a planar discontinuity [*Russell et al.*, 1983]. All four B_Y profiles for O_u have a clearly identified ramp on their earthward side. The end point of the ramp has been used as the benchmark point for time delays between the observations by the four Cluster spacecraft. The resulting wave front normal is $k_{\text{timing}} = [0.54, 0.59, -0.60]$ and forms almost the same angle ($\approx$ 25°) with the separation directions ka_{12} and ka_{14}. Using this method, the velocity of O_u is estimated at 306 km/s. Again, this estimate is very approximate since there is no evidence that the structure is planar. However, all three estimates for the velocity 316 km/s, 245 km/s, and 306 km/s are of the same order of the

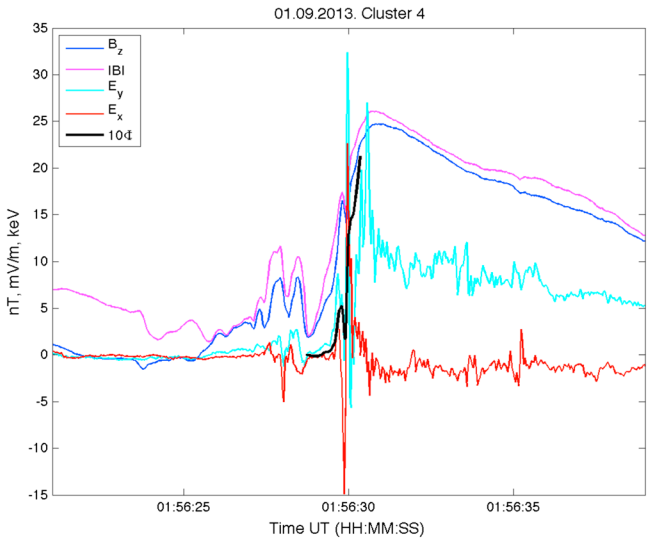

Figure 6. $|B|$ (magenta), B_Z (blue), and E_X (red) as measured by Cluster 4 and the estimate of the change of the electrostatic potential (black) during the observation of DF on 1 September 2003. The electrostatic potential value is increased by a factor of 10 for convenience.

magnitude. If the O_u oscillations are of the same type and origin as O_r, their velocity indicates that the waves may decelerate as they propagate away from the DF. The average time difference for the observation of O_u between the different spacecraft is about 1.5 s, leading to the spatial scale of between 368 km and 465 km.

It is also worth noting that the overall evolution of B_{max}, B_{int}, and B_{min} observed by spacecraft 2 and 3 is similar to that observed by spacecraft 1 and 4 and shown in Figure 3, namely, the occurrence of oscillations in B_{int} around the ramp in B_{max} and finite value of B_{min} (normal component of magnetic field) through the magnetic ramp of the DF.

3.2. Electric Field and Electrostatic Potential Across the DF

Among the four Cluster spacecraft the Cluster 4 electric field data were of the best quality for this DF crossing. Figure 6 displays the modulus of the magnetic field (magenta), B_Z (GSM) component (blue), the E_X (red), and E_Y (light blue) components of the electric field as measured by the EFW instrument together with an estimate of the electrostatic potential Φ (black) across the DF (multiplied by a factor 10). Only two components of the electric field are available from Cluster. Often [e.g., *Fu et al.*, 2012] the condition that the scalar product of electric and magnetic field is zero is used to estimate the third component. However, the validity of this assumption for DFs is not easy to justify. For example, in *Fu et al.* [2012] a significant change in the electron pressure is evident in their Figure 3f. The assumption that the parallel component of the electric field can be neglected may lead to erroneous results if not supported by comprehensive proof that a gradient in the electron pressure along the magnetic field is absent. Such proof is not provided by *Fu et al.* [2012]. The existence of an electron pressure gradient at the DF front is the main reason why only two measured components are presented in the current paper. This is also the reason why the GSE E_Y component is shown in Figure 6 while all other parameters correspond to the GSM frame. Since only two components of the electric field (E_X and E_Y) are available, the estimate of the potential is based on the projection of these components along the average DF normal n_a and assumes a DF propagation velocity of 452.5 km/s as determined by averaging the values above. Since we assume that the motion of the DF is along n_a, the contribution of the $\mathbf{V}\times\mathbf{B}$ terms should be zero for this estimate of the potential. The X component of the electric field exhibits one positive and one negative spike around the time of the local maximum in B_Z and $|B|$. The potential change across the B_Z ramp is about 2 keV. It can also be seen in Figure 6 that a sharp maximum in the magnitude of E_X occurs around the separation at the interface between the increasing and decreasing phase of the B_Y oscillations.

Figure 7 gives a pictorial representation of the relative vector directions discussed in the preceding paragraphs. The reference frame is that resulting from a variance analysis of the DF using Cluster 1 data, with the maximum variance direction vertical and the minimum variance direction normal to the plane of the DF, which is represented by the grey slab. The relative locations of the Cluster satellites are shown such that C1 (black dot) has already encountered the DF and so lies behind it, C3 (green dot) is just beginning its encounter, C4 (blue dot) is just upstream of the DF, and C2 (red dot) lies in front of the DF and is therefore the last satellite to see it. The direction normal to the DF, averaged over all four spacecraft, is shown by the blue arrow (n_a) and represents the direction in which the DF propagates. The red arrow shows the direction of propagation of the O_u oscillations. The green arrows indicate the polarization direction of O_r oscillations.

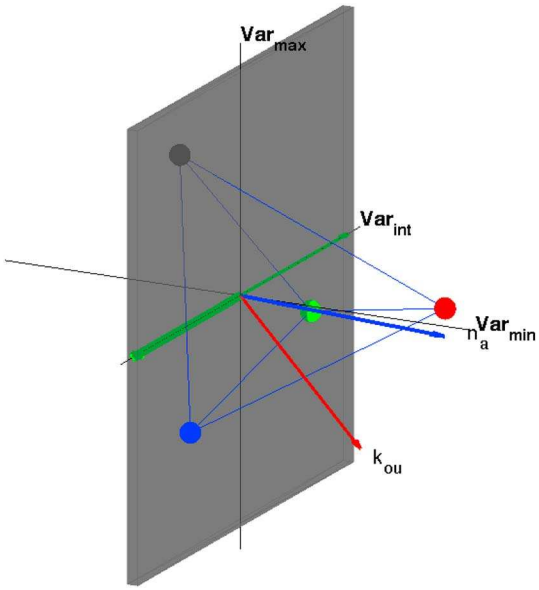

Figure 7. Summary of the DF event observed on 1 September 2003. The grey slab represents the planar orientation of the DF in the variance reference frame defined by the maximum (vertical) and intermediate variance directions based on an analysis of data from Cluster 1. The front propagates along the minimum variance axis. The relative locations of the Cluster tetrahedron are shown such that C1 (black dot) has already encountered the DF and so lies behind it, C3 (green dot) is just beginning its encounter, C4 (blue dot) is just upstream of the DF, and C2 (red dot) lies in front of the DF and is therefore the last satellite to see it. The blue and red arrows represent the normal direction averaged over all four Cluster spacecraft n_a and the propagation direction of the O_u oscillation. The green arrow indicates the polarization direction of the O_r oscillations.

4. DF Event: 12 September 2003 at 18:06 UT

The second event discussed here was observed on 12 September 2003 at around 18:06 UT. The evolution of the B_Z component and the field magnitude $|B|$ are shown in Figure 8 using the same format as Figure 1. During this observation Cluster 1 was located at a position (−107,408, 9689, 14,253) km GSM and traveling in a tailward direction. The spacecraft separation vectors for pairs 1-2, 1-3, and 1-4 were (−128, −200, 80), (49, −214, 124), and (−47, −12, 223) km GSM, respectively. Their relative positions (in the GSE frame) are shown in Figure 9. The arrival of the DF at the Cluster satellites is indicated by the sharp increase in the B_Z component that occurs around 18:06:21 UT for all four spacecraft. For this event, the duration of the main ramp is about 7.8 s (Cluster 1), much longer than that observed in the previous event discussed above. The value of the B_Z component (Figure 8, top), which was close to zero at the beginning of the B_Z ramp, is seen to increase to about 14 nT at the B_Z maximum. The absolute value of the magnetic field (Figure 8, bottom) is about 5 nT at the beginning of the magnetic ramp and reaches a maximum value of 15.5 nT. After the maximum is reached, a gradual decrease in values of B_Z and $|B|$ can be seen in the Figure 8. Once again, local maxima are present within the $|B|$ ramp are clearly visible for all four spacecraft and are also evident in the evolution of B_Z.

4.1. Normal and Velocity of the DF

Once again, the compact nature of the Cluster constellation together with the similarity in the evolution of B_Z and $|B|$ support the assumption of a planar structure for the leading edge of the DF on spatial scales of the spacecraft separation. The magnetic ramps, as observed by all four spacecraft, were subjected to variance analysis to confirm this hypothesis. Data from the entire extent of the magnetic ramp region, as observed by each individual spacecraft, were subjected to a variance analysis. The time intervals that were used for MVA were 18:06:20.27–18:06:32.58, 18:06:21.58–18:06:33.54, 18:06:19.80–18:06:33.27, and 18:06:19.68–18:06:33.32 UT for Cluster 1, Cluster 2, Cluster 3, and Cluster 4, respectively. The minimum variance directions were well defined for all four spacecraft since the ratios of the intermediate to minimum eigenvalues were in the range 19–76. The range of the ratios of the maximum to intermediate eigenvalues was 5–8. The resulting minimum variance directions were very closely aligned to each other, separated by angles in the range 1.6°–7.1°. The minimum variance direction, averaged over the four spacecraft, was $n_a = [0.77, 0.53, -0.35]$ (GSM). The angles between various pairs of maximum variance directions determined from different Cluster spacecraft data were between 0.1° and 1.5°. The close alignment of the minimum and maximum variance directions supports the assumption of planarity of the DF ramp on spatial scales of the spacecraft separation. Assuming that the motion of the leading edge of the DF structure is along the normal n_a, the velocity of the DF has been identified using the spacecraft pairs 1-3 and 2-4. This choice was based on the similarity in the evolution of the magnetic field components through the ramp of the DF. Figure 10 displays three components of the magnetic field in GSM as measured by the Cluster 2 and Cluster 4 spacecraft. Note that the Cluster 2 data have been shifted by −0.65 s which corresponds to the time delay between two spacecraft based on correlation analysis. The good correspondence between all GSM

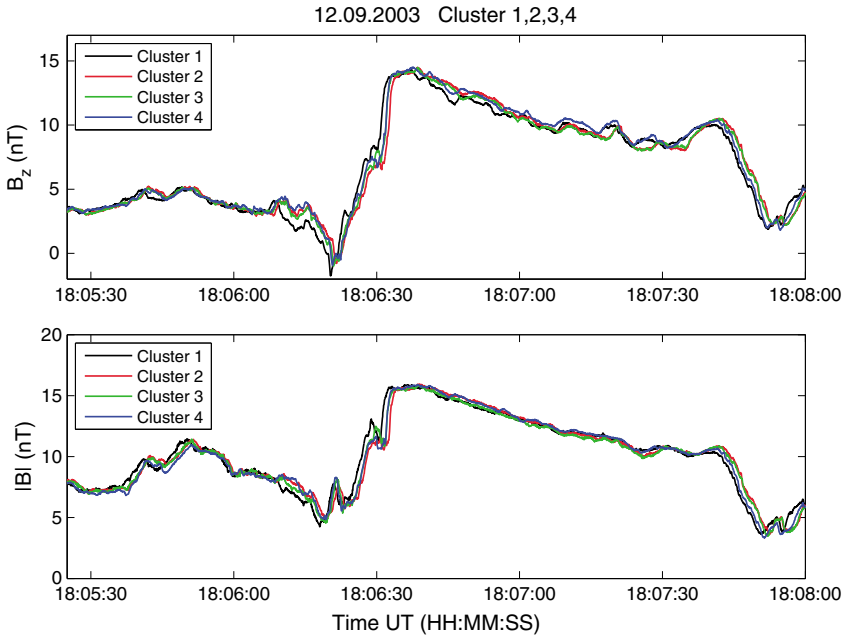

Figure 8. B_Z (GSM) component of (top) the magnetic field and (bottom) the magnetic field magnitude as measured by the four Cluster spacecraft during the time period 18:05:20–18:08:00 UT on 12 September 2003.

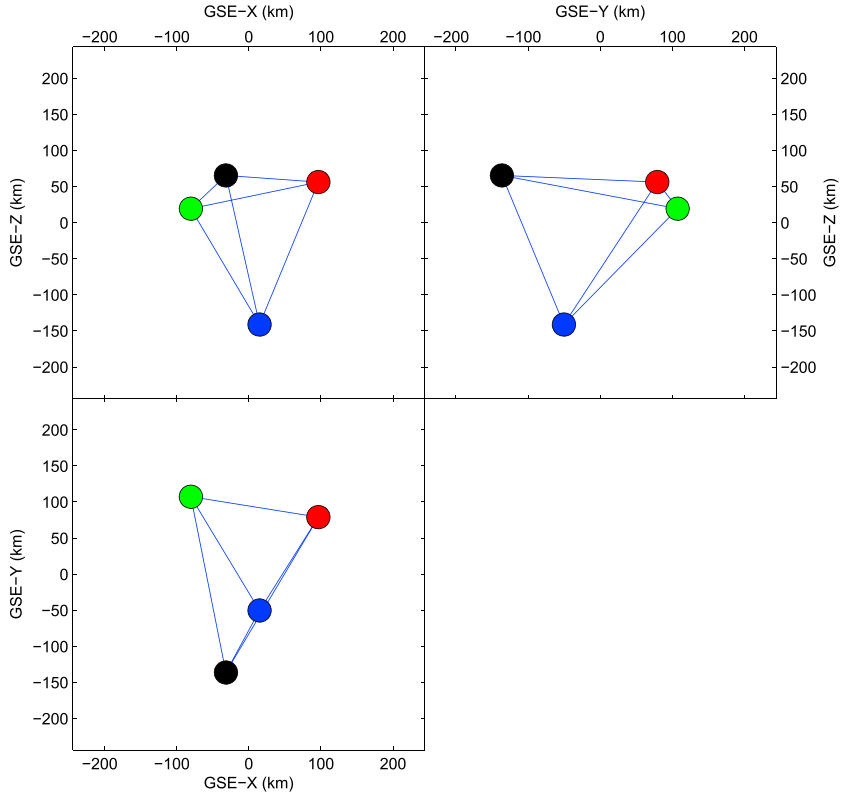

Figure 9. The configuration of the Cluster satellites on 12 September 2003 at 18:06:00.

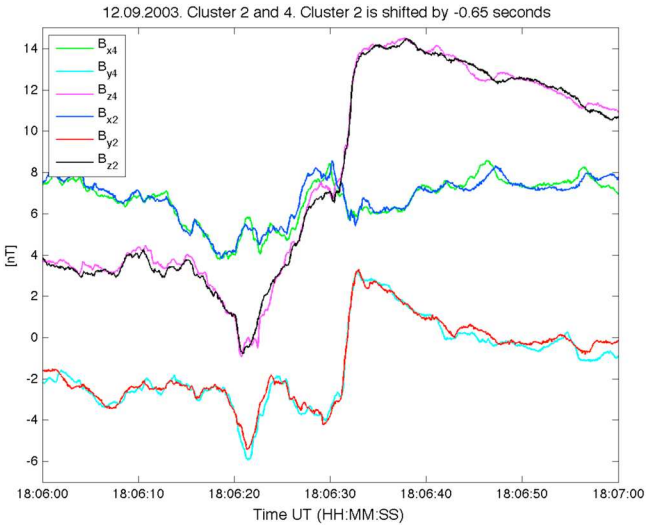

Figure 10. Three components of the magnetic field as measured by Cluster 2 and Cluster 4 during the observation of DF on 12 September 2003. Observations of Cluster 2 are shifted by −0.65 s.

components measured by Cluster 2 and Cluster 4 satellites justifies this value as an estimate for time delay in the observation of the leading edge of DF. The projection of the Cluster 2-Cluster 4 separation vector along the DF normal n_a is 111.5 km, leading to a propagation velocity for the DF of 173 $\pm$ 7 km/s. A similar estimation for the velocity based on measurements from Cluster 1 and Cluster 3 was 158 km/s. The discrepancy between these two estimates is rather small and can be attributed both to the accuracy of n_a and the determination of the time delays. This low velocity explains the longer crossing time of the magnetic ramp for this particular DF.

Figure 11 shows the evolution of $|B|$ and the variance components for Cluster 4. A large oscillation in the B_{int} component in the vicinity of the magnetic ramp is also evident in this event. The nature of this oscillation is similar to that of the previous event discussed above. The evolution of $|B|$ is dominated by the oscillation in B_{int} during the lower part of $|B|$ ramp and by B_{max} at the upper part of the ramp. Cluster 2 also exhibits a similar structure and evolutionary scenario for the magnetic field as is evidenced by the closeness of the variance directions and the almost identical profiles in the GSM components shown in Figure 10. The relative velocity of this DF is significantly slower in comparison to the first event. This leads to the waves having a greater effect on the evolution of the magnetic field normal component, as is evident from Figure 11.

4.2. Electric Field and Electrostatic Potential Across DF

Analysis of the electric field during this event is again based on the measurements from Cluster 4. Figure 12 shows the modulus of the magnetic field, magnetic field B_Z (GSM) component, the E_X, E_Y of the electric field, and an estimate of the electrostatic potential across the front using the same format as Figure 6. For the same reasons as in the first event E_y GSE component is shown. It should be noted that a mean velocity of 165.5 km/s was used for the estimate of the electrostatic potential change. Again, E_X becomes negative during the bottom part of B_Z ramp. However, at the local maximum within the ramp, i.e., during the decreasing phase of oscillation in B_{int}, E_X exhibits large positive maximum, reaching values about 10 mV/m.

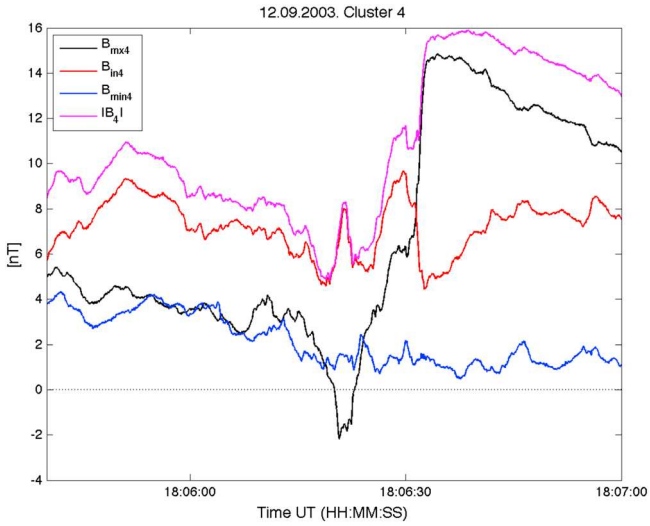

Figure 11. The modulus (magenta) and maximum (black), intermediate (red), and minimum (blue) variance components of the magnetic field during the observation of DF on 12 September 2003.

5. Discussion

It should be noted that while a detailed description and analysis of only two DF events has been presented in this paper, the feature causing the ramp to be non-monotonic is observed within 11/15 of the DF analyzed. Figure 13 shows observations of four other DF seen by Cluster that contain a similar feature which is an implicit indication that oscillations

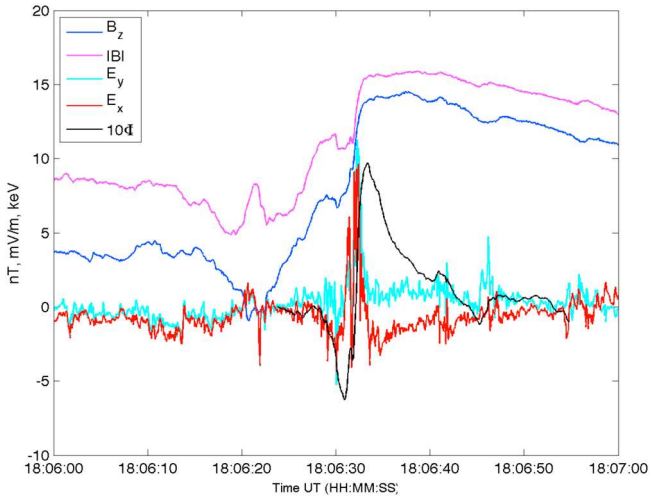

Figure 12. Modulus (magenta) and components of the magnetic field on the maximum (black), intermediate (red), and minimum (blue) variance directions identified from Cluster 4 data during the observation of DF on 12 September 2003.

similar to those discussed above are present. The modulus of the magnetic field and the variance components for one of these events (17 September 2003) are shown in Figure 14. This figure shows that the oscillations in B_{in1} are similar to those observed in events 1 and 2, as discussed above, and that the local maximum in $|B|$ occurs at the turning point between the increasing and decreasing phases of the B_{in1} oscillation. In this particular case the minimum variance component is not so prominent as during the events on 1 and 12 September discussed above. Figure 15 shows the modulus of the magnetic field and the variance components for the DF observed by Cluster 1 on 29 August 2003. This is the same event that has been investigated by *Fu et al.* [2012], and result in the conclusion that "there is no flow of plasma across the DF and that the DF is a tangential discontinuity." In contrast to the other events studied here, this particular event does not exhibit a local maximum within $|B|$. However, the absence of this local maximum does not imply the absence of oscillations in B_{in1}. It may only indicate that these oscillations are not so prominent. The magnetic ramp in both B_Z and $|B|$ is monotonic and does not exhibit any local maximum. However, the oscillation in B_{in1} that occurs around the magnetic ramp is evident during time interval 13:53:13–13:53:16 UT. The absence of its effect on the evolution of $|B|$ within the ramp can be related to the relatively small magnitude (about 2 nT) of the normal component of the magnetic field. This value is significantly lower than for the other three cases presented above. However, this component is nonzero within the ramp of the DF, indicating that in this case the DF cannot be classified as a "tangential discontinuity." The interval used for MVA, 13:53:13.5–13:53:15.64 UT, results in a minimum variance direction (0.18, −0.98, −0.02) which is almost aligned along the *Y* GSM axis. This indicates either that the local disturbance of the DF is similar to the corrugation instability caused by rippling of the DF or that a flank of the DF is observed. The latter is in accordance with the position of Cluster (17.5, −1.8, 2.8) R_e (GSM). The ratios

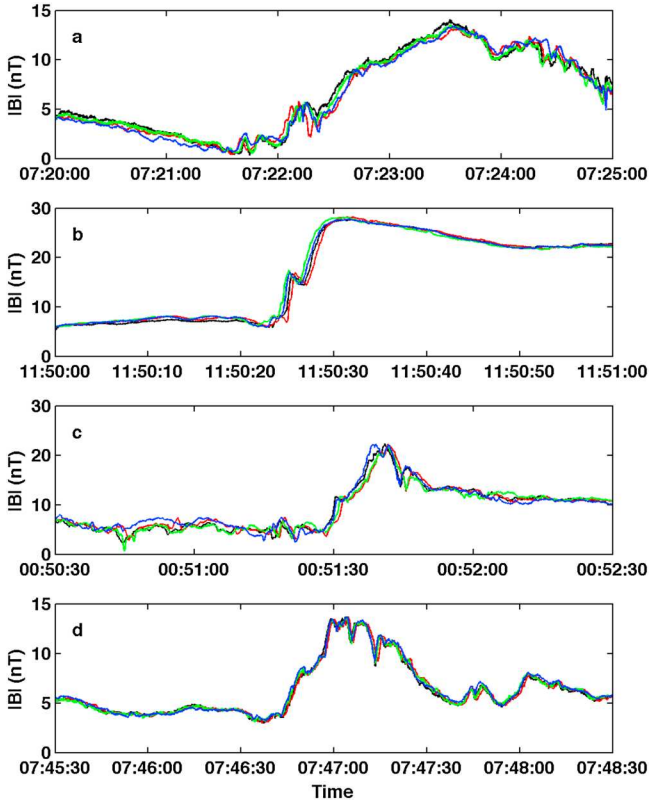

Figure 13. Modulus of the magnetic field for four dipolarization fronts observed by the four Cluster spacecraft (Cluster 1, black; Cluster 2, red; Cluster 3, green; Cluster 4, blue) on (a) 20 August 2003, (b) 17 September 2003, (c) 2 October 2003, and (d) 11 October 2003.

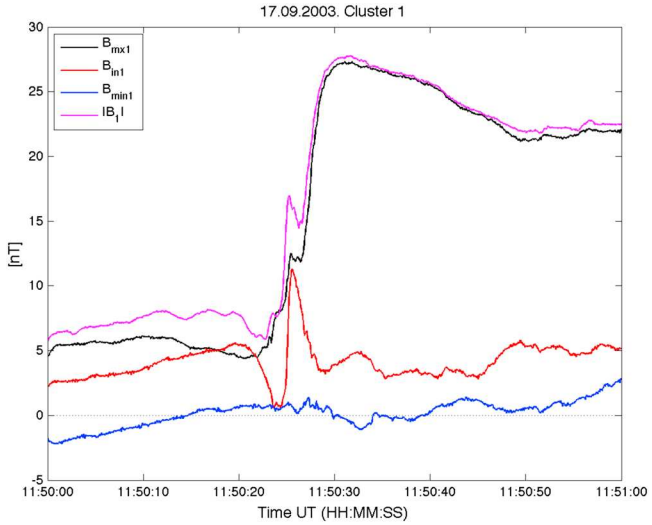

Figure 14. Modulus (magenta) and components of the magnetic field on the maximum (black), intermediate (red), and minimum (blue) variance directions identified from Cluster 1 data during the observation of DF on 17 September 2003.

between the minimum, intermediate, and maximum eigenvalues are 1:37:815. The estimate of the statistical error in the normal component of the magnetic field, according to the methodology of *Sonnerup and Scheible* [1998], is about 0.4 nT. As was explained above, the disregard of the electron pressure gradient that is required to estimated the third unmeasured component of the electric field can lead to erroneous results. Figure 15 presents another disagreement with the results of *Fu et al.* [2012] who used the timing between the four spacecraft to identify the DF normal direction. According to their result, the normal direction is (0.61, −0.70, 0.36) (GSM). The angle between the MVA normal for Cluster 1 and the timing normal determined by *Fu et al.* [2012] is about 50°. The projection of the magnetic field along this timing normal direction B_{nF} is plotted in Figure 15 (cyan). It can be seen from this figure that this projection undergoes a significant variation during the first part of the magnetic ramp. Overall, the change of the magnetic field magnitude (magenta line) in this DF is about 10.2 nT. During the first part of the ramp, in which the magnetic field magnitude changes by about 3.04 nT, the value of B_{nF} changes by +1.93 nT, or about 64% of the magnetic field magnitude change, and also changes sign in the process. The calculations performed by *Fu et al.* [2012] to show the absence of the vanishing tangential electric field component are very sensitive to the direction of the normal and the assumption of DF planarity on spacecraft separation scales. The significant variation of B_{nF} indicates that the timing normal identified by *Fu et al.* [2012] is not valid at least for the Cluster 1 spacecraft and undermines further estimations of the tangential component of the electric field and hence the main conclusion of *Fu et al.* [2012]. The minimum variance component of the magnetic field does not exhibit significant variation within the ramp of the DF and possesses finite value of about 2 nT. The existence of the nonzero normal component in the events observed by Cluster on 1 September and 29 August 2003 proves that the structures observed cannot be classified as tangential discontinuities. However, this raises the following question: How large does B_{min} need to be in order to allow particle motion across the DF? Any plasma particle can move freely along the magnetic field line if its energy exceeds the corresponding part of electrostatic potential. Since the normal component represents only part of the total magnetic field, the charged particle penetration distance L_n along the normal, while moving along the field line, requires a corresponding

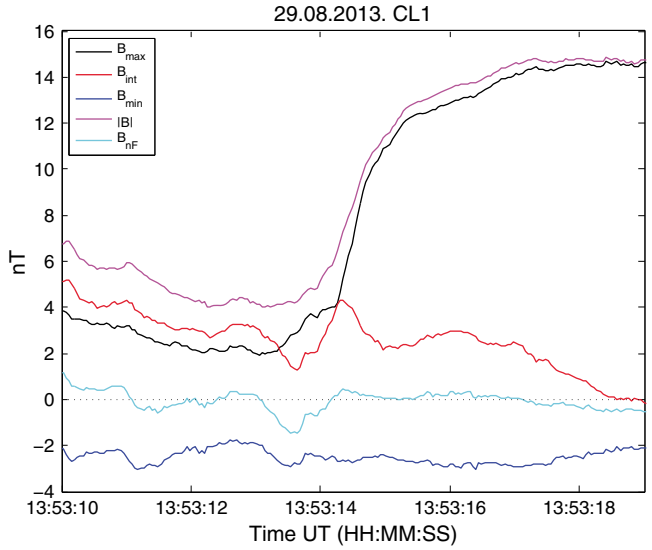

Figure 15. Modulus (magenta) and components of the magnetic field on the maximum (black), intermediate (red), and minimum (blue) variance directions identified from Cluster 1 data during the observation of DF on 29 August 2003. Cyan line corresponds to the projection of the magnetic field along the direction identified as normal in *Fu et al.* [2012].

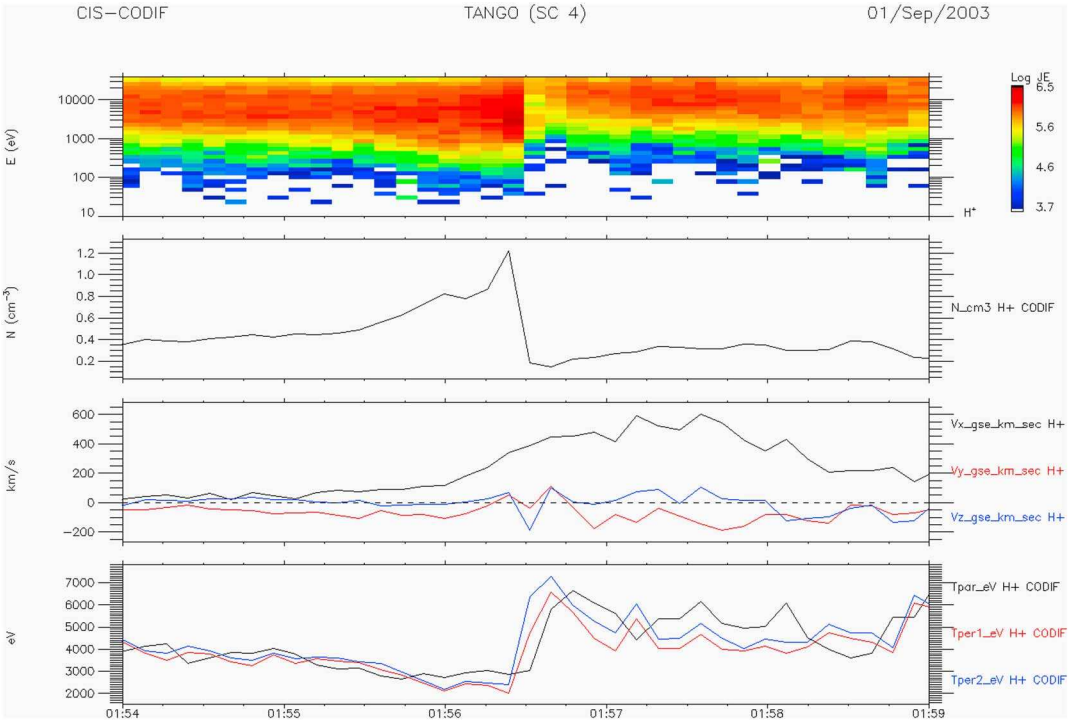

Figure 16. CIS parameters for the DF observed on 1 September 2003.

displacement in the tangential plane L_t. The order of the magnitude of L_t can be estimated as $\frac{\langle B_t \rangle}{\langle B_n \rangle} L_n$, where $\langle\rangle$ means averaging and B_t, B_n are the tangential and normal components of the magnetic field. In case of the DF observed on 1 September 2003, the width of the $|B|$ ramp is 571 km. Since this is a very rough estimate, the assumption from Figure 3 that $\frac{\langle B_t \rangle}{\langle B_n \rangle} \approx 12.5$ leads to $L_t \approx 7000$ km. This value is lower than the spatial scales of DFs in "dawn-dusk" and "north-south" directions [*Nakamura et al.*, 2004]. This implies that at least some particles can cross this DF.

The propagation velocities identified for the DF discussed above can be used to estimate the spatial scales of the magnetic ramp region of the DFs. For the DF observed on 1 September 2003 the duration of the B_Z and $|B|$ magnetic ramps observed by Cluster 1 are about 0.76 and 1.26 s, respectively. Based on a propagation velocity of 453 km/s, these times lead to the estimates of $L_{Bz} = 344$ km and $L_{|B|} = 571$ km for their spatial scales. Figure 16 displays the moments of the ion distribution obtained by the CIS-CODIF sensor onboard Cluster 4. In the region just upstream of the DF the perpendicular ion temperature is about 3 keV and increases to a value of around 7 keV at the top end of the magnetic ramp. During this period, the modulus of the magnetic field increases from around 1.8 nT just upstream of the ramp to a value 24 nT at the end of the ramp. Using these values, the Larmor radius R_L of the thermal ions can be estimated as $R_{Lb} \approx 3100$ km just upstream of the bottom of the ramp and $R_{Lt} \approx 355$ km at its top end. In the middle of the ramp, taking the mean magnetic field and ion temperature as 13 nT and 5 keV, the Larmor radius was estimated to be $R_{Lm} \approx 555$ km. Since all of these estimates for R_L exceed the spatial scale of the B_Z ramp, they should be treated as formally calculated numbers rather than characteristics of the ion motion. The spatial scales of the leading edge of the DF can therefore be expressed as

$$L_{Bz} = 0.11R_{Lb} = 0.62R_{Lm} = 0.97R_{Lt}$$

$$L_{|B|} = 0.18R_{Lb} = 1.03R_{Lm} = 1.60R_{Lt}.$$

The time durations of the increases in B_Z and $|B|$ observed by Cluster 1 for the DF on 12 September 2003 are 7.5 and 7.8 s. The mean propagation velocity of 165 km/s leads to scale estimates of $L_{Bz} = 1238$ km and $L_{|B|} = 1287$ km, respectively. Figure 17 shows the moments of the ion distribution obtained by the CIS-CODIF sensor onboard Cluster 4 during the time interval 18:04–18:09 UT. In the vicinity of the magnetic

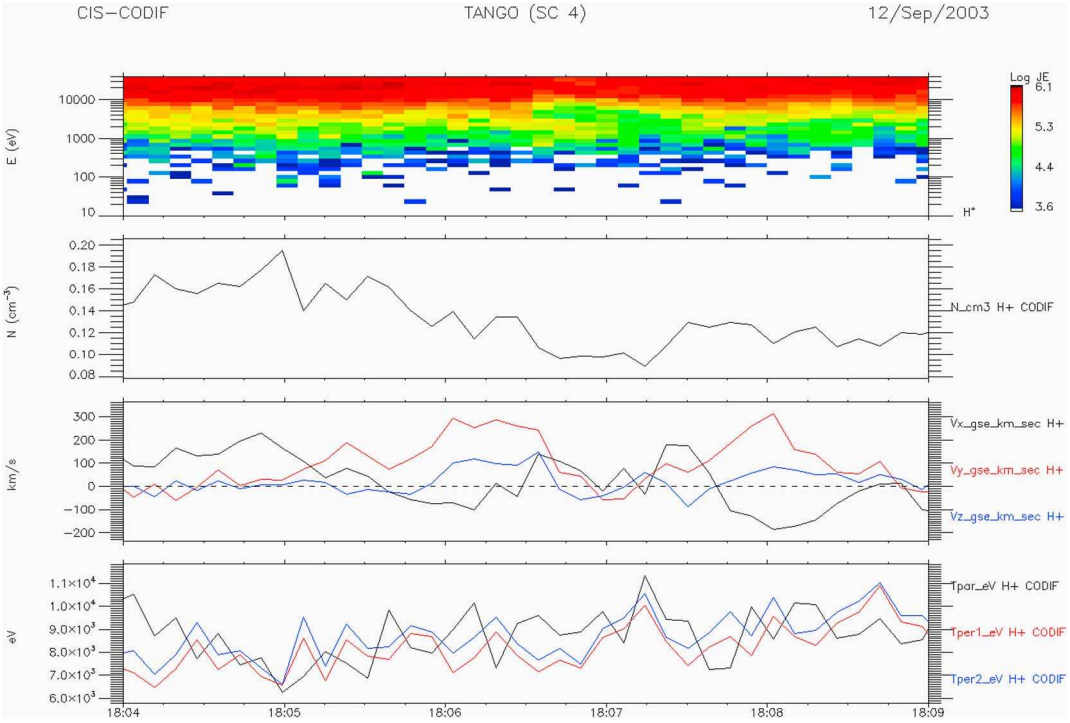

Figure 17. CIS parameters for the DF observed on 12 September 2003.

ramp, the perpendicular temperature varies between about 7.5 keV and 9.5 keV, and the mean value (8.5 keV) has been used to estimate the gyroradius. This estimate should be accurate enough for our purposes since the gyroradius only depends upon $\sqrt{T}$. Based on the variation of magnetic field magnitude observed by Cluster 1 at the beginning (~6.4 nT) and end (~15.6) nT of the ramp, the corresponding Larmor radii were estimated as $R_{Lb} \approx 1470$ km, $R_{Lm} \approx 855$ km, and $R_{Lt} \approx 603$ km. These values lead to spatial scales for the leading edge of this DF of

$$L_{Bz} = 0.84R_{Lb} = 1.44R_{Lm} = 2.05_{Lt}$$

$$L_{|B|} = 0.88R_{Lb} = 1.5R_{Lm} = 2.13R_{Lt}.$$

For the DF observed on 1 September the spatial scale of the B_Z ramp is less than the estimates of the Larmor radius corresponding to either the bottom or center of the magnetic ramp approximately equal to that for the top of the ramp. It is currently accepted that the pressure of the magnetic field behind the magnetic ramp of the DF is balanced by the plasma thermal pressure in front of the ramp. In the absence of a significant contribution from the electrostatic potential, the typical scale at which the ion distribution undergoes modification is of the order of R_L for a magnetized plasma. It can be seen from Figure 1 that the field at the local maximum observed in the middle of the B_Z magnetic ramp has increased about 5 times with respect to the pre-DF value, leading to an increase in the magnetic pressure of ~25 times. At the same time the electrostatic potential has increased by less than 500 V. This value corresponds to an energy that is only a small fraction of the ion temperature. As was discussed above in relation to Figure 4, the oscillation in B_{int} results in a widening of the spatial scale over which the modulus of the magnetic field, and therefore the magnetic pressure, increases. This leads to a larger spatial scale in which the plasma pressure should undergo readjustment in order to maintain pressure balance. Similar physical effects have been observed in laboratory experiments on current sheet formation [*Frank et al.*, 2009] and intense current sheets in the magnetotail [*Artemyev et al.*, 2013]. The effect of these oscillations on the pressure balance does not explain the physical mechanism for the generation of these oscillations. The effective spatial scale of O_u is between 368 km and 465 km. As can be seen from Figure 16 the ion density from Cluster 4 is about 0.8 cm^{-3}. Thus, in terms of the ion inertial length c/ω_{pi} the scale is between $1.4c/\omega_{pi}$ and $1.8c/\omega_{pi}$. The average magnetic field

in the regions adjacent to the O_u oscillation from the earthward side have been calculated for each spacecraft. The average field directions for spacecraft 1, 2, and 3 are similar to each other, with angular variations in the range 10°–16°. However, the direction of the magnetic field identified from spacecraft 4 forms angles of 20°, 30°, and 37° with those identified from the other three spacecraft. This can be explained by the fact that Cluster 4 is largely separated from the other spacecraft along the GSM Z direction. The magnetic field averaged for the Cluster 1, Cluster 2, and Cluster 3 spacecraft is (0.66, 3.12, 2.10) nT and its magnitude 3.8 nT. These values of $|B|$, combined with the density and temperature, correspond to an Alfvén velocity $v_a = 93$ km/s and the proton thermal velocity $v_{Ti} = 536$ km/s. The best particle data for this time interval are available from Cluster 4. The separation between Cluster 4 and other spacecraft is in the range 212–238 km which is significantly less than the proton Larmor radius and so can be used for the other three spacecraft as well. It is difficult to relate the velocity of O_r oscillations in B_{in} to Alfvénic or thermal velocities because of the drastic change in the plasma parameters at the ramp of the observed DFs. However, if it is assumed that the O_u oscillations observed on 1 September are of the same type as O_r, it is possible to use O_u to relate the speed of these oscillations to the characteristic plasma velocities. The time resolution of the CIS instrument is insufficient to determine the plasma bulk velocity that corresponds exactly to the interval in which O_u is observed. From Figure 16 it is evident that the plasma bulk velocity is directed almost along X axis and changes from about 350–400 km/s. This corresponds to the ranges 213–244 km/s and 193–221 km along the ka_{12} and ka_{14} directions, respectively. The angles of ka_{12} and ka_{14} to the averaged magnetic field are 80° and 81° correspondingly. The phase velocity of linear Alfvén waves along ka_{12} and ka_{14} would be 14 km/s and 16 km/s, respectively. Taking into account the direction of propagation with respect to the magnetic field and the ratio of the Alfvén and thermal ion velocities v_a/v_{Ti}, it is easy to show that the phase velocity of the linear fast magnetosonic wave will be close to v_{Ti}. Therefore, in spite of the low accuracy for the wave speed determination it can be concluded that O_u propagates with a velocity that is much closer to that of a small amplitude Alfvén wave propagating in the same direction. Obviously, O_u is a highly nonlinear structure with $\delta B/B_0 > 1$ and cannot be treated as a linear wave.

A number of physical mechanisms can lead to such variations in the magnetic field. The first probable mechanism is based on the so-called electron curvature current that occurs due to an anisotropy in the electron pressure. It was suggested that the electron curvature current leads to similar magnetic field variations and a widening of the magnetic pressure gradient for intense current sheets [*Artemyev et al.*, 2013] or laboratory experiments of current sheet formation [*Frank et al.*, 2009]. Under the assumption of planarity the generalized Ohms law expressed in a coordinate frame in which the X, Y, and Z axes correspond to the minimum, intermediate, and maximum variance directions can be written as

$$\nabla \hat{p}_e = -en_0\mathbf{E} + \frac{1}{c}\left[\mathbf{j}_e \times \mathbf{B}\right], \tag{3}$$

where $\mathbf{j}_e$ and $\nabla \hat{p}_e$ are the electron current and the electron pressure tensor

$$\nabla \hat{p}_e = \nabla_\perp p_{\perp e} + \nabla_\parallel p_{\parallel e} + \Lambda\left((\mathbf{B}\nabla)\,\mathbf{B} - 2\frac{\mathbf{B}}{B}(\mathbf{B}\nabla)\,B\right), \tag{4}$$

and $\Lambda = \left(p_{\parallel e} - p_{\perp e}\right) B^2$.

If all variations of $\mathbf{B}$ occur along the normal to the planar structure, then $\partial_x, \partial_y = 0$ and $\partial_x B_x = 0$. However, when all parameters exhibit variations in the X (minimum variance) direction, any oscillations in the magnetic field observed in the Y (intermediate variance) direction are related to the current along Z (maximum variance direction). After substitution of (2) into (1) and considering the Z component of the resulting equation, an expression for j_{ez} can be easily found:

$$j_{ez} = \frac{c\Lambda}{B^2}\left(\left(B^2 - 2B_y^2\right)\partial_x B_y - 2B_y B_z \partial_x B_z\right). \tag{5}$$

It is beneficial to further investigate the three terms of (5) that correspond to the field structure based on the observations by Cluster. From Figure 3 it can be seen that in the initial stage of the oscillation O_r (around 01:56:29 UT), the modulus of the magnetic field (magenta) is determined mainly by the contribution from the magnetic field component along the intermediate variance direction (red). If the X axis is directed toward the Earth, both $\left(B^2 - 2B_y^2\right)$ and $\partial_x B_y$ are negative and therefore the first term in brackets in (3) is positive. The second term is also positive because $\partial_x B_z$ is negative. Therefore, the sign of j_{ez} is determined by Λ.

In the tail, earthward of the DF, Λ is positive (since $p_{\|e} > p_{\perp e}$) and so j_{ez} should also be positive. In such a case B_Y should have a positive gradient according to Maxwell's equation:

$$\frac{\partial B_y}{\partial x} = \frac{4\pi}{c} j_z.$$

However, if, as in the above calculations, X is directed toward the Earth, $\partial B_y/\partial x$ is negative (see Figure 3). Therefore, an electron curvature current cannot explain the observed field structure.

A second explanation for the origin of these oscillations can be attributed to the various instabilities observed at the leading edge of a DF. Various analytical, observational, and numerical studies have addressed these plasma instabilities observed in the vicinity of a DF. The majority of these studies consider lower hybrid drift (LHD) and whistler waves. However, both types of waves are observed at significantly higher frequencies than the oscillations that are considered here. Whistler waves [*Khotyaintsev et al.*, 2011] are observed in the range of 10^2 Hz inside the pileup region. LHD waves are observed at the leading edge of a DF, at the same place in which the oscillations in the intermediate component discussed above are observed, but their frequency is significantly (around 5–15 times) higher. The low frequency of the oscillation shown in Figures 5 and 12, together with the absence of a corresponding variation in the electric field component, implies, with a high level of confidence, that these waves are not related to the LHD instability. A number of numerical studies have been devoted to the development of the interchange instability in the vicinity of DFs [*Pritchett and Coroniti*, 2010, 2011; *Vapirev et al.*, 2013]. *Vapirev et al.* [2013] demonstrated the formation of "finger-like density structures." However, the characteristic timescales for the field variations associated with these structures are close the lower hybrid frequency (in excess of 10 Hz for both DF discussed here). The spatial scales, typical frequencies, and polarization of the oscillations observed by Cluster are also substantially different from waves resulting from the kinetic ballooning instability investigated in numerical simulations [*Pritchett and Coroniti*, 2010, 2011]. The polarization of the dominant mode observed in numerical studies lies in the direction parallel to the magnetic field, and, therefore, within the ramp the polarization of the observed waves should have the significant component along the maximum variance direction, especially downstream of the B_{in} maximum. However, in the Cluster data presented the oscillations are observed in the intermediate variance component.

Figure 4 offers a possible explanation of the origin for these oscillations. As mentioned above, the variation of B_{int} observed within the ramp forms part of a set of oscillations observed upstream of the DF. One of the classical problems regarding the physics of shocks in an ordinary gas or plasma is related to a disturbance caused by a moving piston. For a collisional gas the instantaneous motion of a piston, even at subsonic speeds, will result in the formation of a shock wave ahead of the piston. As was shown in the classical shock physics textbook by *Zeldovich and Raizer* [1966], the condition of "instantaneous motion" is not required for shock formation. For a gradual acceleration of the piston a shock will be formed some time after and at some distance from the piston location. In the case of a medium that is governed by the MHD equations, the problem is similar to that involving the motion of a piston in ordinary gas, a configuration that has also been comprehensively investigated. It was shown that for cases involving either a pressure pulse or the motion of a conducting plane fast and slow shocks, Alfvénic discontinuities and some other disturbances can be formed ahead of the piston [e.g., *Akhiezer et al.*, 1975]. Obviously these MHD and gas dynamic problems are not directly applicable to the motion of a DF that possesses finite spatial scales in the Z and Y directions. However, since the motion of the DF is slower than thermal velocity (and also the fast magnetosonic speed), it will excite eigenmodes of the plasma and therefore lead to disturbances upstream. The composition of eigenmodes excited by the motion of a piston is rather complex and depends upon the boundary conditions at the piston surface, the velocity of its motion, and its orientation with respect to the magnetic field. Even in a significantly simpler case of instantaneous piston motion in the uniform medium governed by the MHD equations the motion of the piston can lead to various combinations of fast and slow magnetosonic shocks, automodel waves, and Alfvén discontinuities. The determination of the exact combination of possible waves that can be generated by the motion of a DF in a much more complex system of magnetotail plasma is beyond scope of the present study.

Finally, it must be noted that the oscillations in B_{int} that occur around the magnetic ramp indicate the presence of an electric current flowing along the maximum variance direction, which is close to the magnetic field direction at the top of the ramp. The magnitude of this field-aligned current can be estimated using $\text{curl}\, B = \mu_0 j$ using the amplitude of the oscillations and spatial scale of the magnetic ramp. From Figure 3

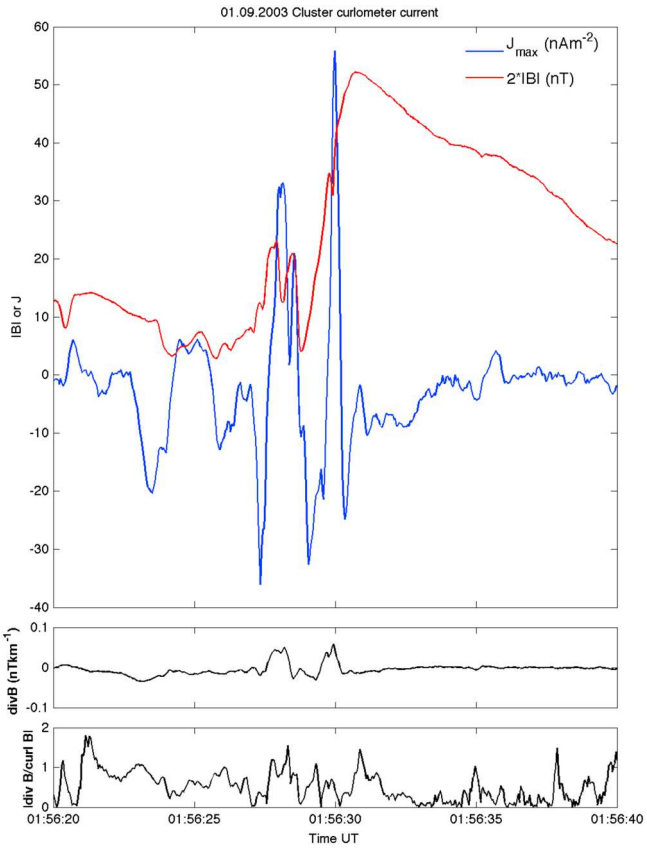

Figure 18. (first panel) Current in the maximum variance direction (blue) together with the magnitude of the magnetic field $|B|$ (red), calculated using the curlometer technique, for the DF observed on 1 September 2003. (second and third panels) The div B and div B/curl B that provide some estimation of the quality of the current calculated using the curlometer.

(the 1 September event) it is seen that the change in B_{int} from the maximum observed within the first half of the ramp to the following minimum is about ΔB =~14 nT. The spatial scale over which this change occurs is about half of the magnetic ramp width, so $\Delta L \sim$ 280 km. The order of magnitude estimate of the field-aligned current density $J \sim \Delta B/(\Delta L \mu_0) = 40\,\mathrm{nA\,m^{-2}}$. The curlometer technique [*Dunlop et al.*, 2002] also can be used to identify the electric current using the magnetic field data from all four spacecraft. The magnitude of the electric current density determined using this methodology is shown in Figure 18 (first panel). The maximum of the current density is about 60 nA m^{-2}. Its value, averaged over the same region that was used for the analytical estimate, is close to 40 nA m^{-2}. However, in spite of the close similarity between these two values, the analytical estimate and curlometer result should be treated as order of magnitude estimates only, the first because of the oversimplified geometry used by replacing curl B with $\Delta B/\Delta L$, and the second (curlometer) because the quality parameters div B and div B/curl B [*Robert et al.*, 1998] both deviate from zero as shown in Figure 18 (second and third panels). Thus, it seems that the field-aligned current is the most plausible explanation of these oscillations in the magnetic ramp. However, it is not straightforward to apply the same explanation to O_u oscillation in Figure 5.

An unexpected feature that can be seen in Figures 6 and 12 is the negative direction of the electric field and the corresponding changes in the electrostatic potential during the initial part of magnetic ramp. It should be noted that (as mentioned above) the electrostatic potential plotted in Figures 6 and 12 is just an estimate that is based on the two component measurements available from Cluster. A complete 3-D measurement of the electric field is required to investigate the actual evolution of the electric potential within the DF. These figures also illustrate that the electric field undergoes sharp changes on the scales that are even shorter than the width of the magnetic ramp. It is known from the shock studies that steep gradients of the electric field can lead to the demagnetization of the electrons. The electric field data displayed in Figures 6 and 12 also enable the investigation of whether the gradient in the electric field within the DF is strong enough to lead to the effective demagnetization of electrons. The demagnetization of electrons in an electromagnetic field structure typical of a quasi-perpendicular collisionless shock front is discussed by *Balikhin et al.* [1993, 1998], *Balikhin and Gedalin* [1994], and *Gedalin et al.* [1995]. It is shown that gradient of the electric field leads to the change of the electron gyration frequency. If the gradient is strong enough and the gyration frequency approaches zero, the transition from the gyrating motion to the motion along the rectified trajectories takes place. It is this transition in the electron motion that is referred to in *Gedalin et al.* [1995] and *Balikhin et al.* [1998] as the demagnetization. Demagnetization occurs when

$$\frac{e}{m\Omega_{Be}^2}\left|\frac{\partial^2\Phi}{\partial x^2}\right| - 1 > 0,$$

where Ω_{Be} is the electron Larmor frequency and Φ is the cross-shock potential. The steepest part of the electrostatic potential increase for the DF observed on 1 September 2003 takes place at the top part of the magnetic ramp, just after the local maximum discussed above. The estimate of the electrostatic potential there changes by 1120 V in approximately 0.08 s. The electron Larmor frequency during this interval is about $\Omega_{Be} \approx 2640$ rad/s. Assuming that the velocity of Cluster 4 with respect to the DF is 452 km/s, it is easy to estimate that $\frac{e}{m\Omega_{Be}^2}\left|\frac{\partial^2\Phi}{\partial x^2}\right| \approx 2.2 \cdot 10^{-2}$. Therefore, the electric field gradients are too weak to lead to electron demagnetization at the DF. It is worth noting that even when the electric field gradients are too weak to reach the demagnetization threshold, the deviation in the electron dynamics from the standard drift motion can still occur due to the change in the effective gyration frequency.

6. Conclusions

In this paper it has been shown that, at least for some DF, in addition to a sharp increase in the maximum variance magnetic field component (that is close to *Z* GSM), significant oscillations in the perpendicular intermediate variance component (close to *Y* GSM) are taking place. These oscillations can lead to a widening of the spatial scale of the magnetic pressure gradient and therefore is essential in maintaining the pressure balance within the DF. A number of physical mechanisms were considered in order to determine the formation of these oscillations. The evolution of the magnetic field can rule out the electron curvature current that has been proposed to explain similar effects in intense current sheets. Various local instabilities could be responsible for the occurrence of these oscillations. However, instabilities leading to lower hybrid drift waves, such as the interchange instability, should be ruled out due to the significant difference between the spatial and temporal scales of the observed oscillations and lower hybrid drift waves. It is possible that the formation of these oscillations in the region upstream of the DF is similar to the formation of disturbances and even shock waves as the result of a sudden or gradual acceleration of a pressure pulse in classical hydrodynamics and magnetohydrodynamics. The subsonic motion of some disturbance in any media usually leads to waves (corresponding to the eigenmodes of this media) propagating away. Oscillations observed within the magnetic ramp indicate field-aligned currents that are expected to be associated with DF.

The investigation of the electric field gradients within the DF shows that in the cases studied these gradients are too weak to cause the demagnetization of electrons. Finally, the bipolar-type variations of the electric field within the front have not been observed before but still requires a confirmation by measurements when all three components of the electric field are available.

Acknowledgments

M.A.B. would like to acknowledge financial support from ISSI, EPSRC, STFC, and The Royal Society. A.R. acknowledges funding from NASA grant NNX13AF81G. M.A.B. would like to thank A. Artemyev H. Fu for useful discussions. The data used in this study are available from the Cluster Active Archive.

Larry Kepko thanks the reviewers for their assistance in evaluating this paper.

References

Akhiezer, A. I., I. A. Akhiezer, R. V. Polovin, A. G. Sitenko, and K. N. Stepanov (1975), *Plasma Electrodynamics*, Pergamon Press, Oxford, U. K.

Angelopoulos, V., W. Baumjohann, C. F. Kennel, F. V. Coroniti, M. G. Kivelson, R. Pellat, R. J. Walker, H. Lühr, and G. Paschmann (1992), Bursty bulk flows in the inner central plasma sheet, *J. Geophys. Res.*, *97*, 4027–4039, doi:10.1029/91JA02701.

Angelopoulos, V., A. Runov, X.-Z. Zhou, D. L. Turner, S. A. Kiehas, S.-S. Li, and I. Shinohara (2013), Electromagnetic energy conversion at reconnection fronts, *Science*, *341*, 1478–1482, doi:10.1126/science.1236992.

Artemyev, A. V., S. Kasahara, A. Y. Ukhorskiy, and M. Fujimoto (2013), Acceleration of ions in the Jupiter magnetotail: Particle resonant interaction with dipolarization fronts, *Planet. Space Sci.*, *82*, 134–148, doi:10.1016/j.pss.2013.04.013.

Balikhin, M., and M. Gedalin (1994), Kinematic mechanism of electron heating in shocks: Theory vs observations, *Geophys. Res. Lett.*, *21*, 841–844, doi:10.1029/94GL00371.

Balikhin, M., M. Gedalin, and A. Petrukovich (1993), New mechanism for heating in shocks, *Phys. Rev. Lett.*, *70*, 1259–1262, doi:10.1103/PhysRevLett.70.1259.

Balikhin, M. A., V. Krasnoselskikh, L. J. C. Woolliscroft, and M. Gedalin (1998), A study of the dispersion of the electron distribution in the presence of *E* and *B* gradients: Application to electron heating at quasi-perpendicular shocks, *J. Geophys. Res.*, *103*(A2), 2029–2040, doi:10.1029/97JA02463.

Balogh, A., et al. (1997), The Cluster magnetic field investigation, *Space Sci. Rev.*, *79*, 65–91, doi:10.1023/A:1004970907748.

Dunlop, M. W., A. Balogh, K.-H. Glassmeier, and P. Robert (2002), Four-point Cluster application of magnetic field analysis tools: The Curlometer, *J. Geophys. Res.*, *107*(A11), 1384, doi:10.1029/2001JA005088.

Frank, A., S. Bugrov, and V. Markov (2009), Enhancement of the guide field during the current sheet formation in the three-dimensional magnetic configuration with an X line, *Phys. Lett. A*, *373*, 1460–1464, doi:10.1016/j.physleta.2009.02.037.

Fu, H. S., Y. V. Khotyaintsev, M. André, and A. Vaivads (2011), Fermi and betatron acceleration of suprathermal electrons behind dipolarization fronts, *Geophys. Res. Lett.*, *38*, L16104, doi:10.1029/2011GL048528.

Fu, H. S., Y. V. Khotyaintsev, A. Vaivads, M. André, and S. Y. Huang (2012), Electric structure of dipolarization front at sub-proton scale, *Geophys. Res. Lett.*, *39*, L06105, doi:10.1029/2012GL051274.

Gedalin, M., K. Gedalin, M. Balikhin, V. Krasnosselskikh, and L. J. C. Woolliscroft (1995), Demagnetization of electrons in inhomogeneous $E_\perp B$: Implications for electron heating in shocks, *J. Geophys. Res.*, *100*, 19,911–19,918, doi:10.1029/95JA01399.

Gustafsson, G., et al. (1997), The electric field and wave experiment for the Cluster mission, *Space Sci. Rev.*, *79*, 137–156.

Khotyaintsev, Y. V., C. M. Cully, A. Vaivads, M. André, and C. J. Owen (2011), Plasma jet braking: Energy dissipation and nonadiabatic electrons, *Phys. Rev. Lett.*, *106*(16), 165001, doi:10.1103/PhysRevLett.106.165001.

Liu, J., V. Angelopoulos, A. Runov, and X.-Z. Zhou (2013), On the current sheets surrounding dipolarizing flux bundles in the magnetotail: The case for wedgelets, *J. Geophys. Res. Space Physics*, *118*, 2000–2020, doi:10.1002/jgra.50092.

Nakamura, M. S., H. Matsumoto, and M. Fujimoto (2002a), Interchange instability at the leading part of reconnection jets, *Geophys. Res. Lett.*, *29*, 1247–1250, doi:10.1029/2001GL013780.

Nakamura, R., et al. (2002b), Motion of the dipolarization front during a flow burst event observed by Cluster, *Geophys. Res. Lett.*, *29*(20), 1942, doi:10.1029/2002GL015763.

Nakamura, R., et al. (2004), Spatial scale of high-speed flows in the plasma sheet observed by Cluster, *Geophys. Res. Lett.*, *31*, L09804, doi:10.1029/2004GL019558.

Ohtani, S.-I., M. A. Shay, and T. Mukai (2004), Temporal structure of the fast convective flow in the plasma sheet: Comparison between observations and two-fluid simulations, *J. Geophys. Res.*, *109*, A03210, doi:10.1029/2003JA010002.

Pedersen, A., et al. (1997), The wave experiment consortium (WEC), *Space Sci. Rev.*, *79*, 93–106.

Pritchett, P. L., and F. V. Coroniti (2010), A kinetic ballooning/interchange instability in the magnetotail, *J. Geophys. Res.*, *115*, A06301, doi:10.1029/2009JA014752.

Pritchett, P. L., and F. V. Coroniti (2011), Plasma sheet disruption by interchange-generated flow intrusions, *Geophys. Res. Lett.*, *38*, L10102, doi:10.1029/2011GL047527.

Rème, H., et al. (2001), First multispacecraft ion measurements in and near the Earth's magnetosphere with the identical Cluster ion spectrometry (CIS) experiment, *Ann. Geophys.*, *19*, 1303–1354.

Robert, P., A. Roux, C. C. Harvey, M. W. Dunlop, P. W. Daly, and K.-H. Glassmeier (1998), Tetrahedron geometric factors, in *Analysis Methods for Multi-Spacecraft Data, ISSI Scientific Report*, vol. SR-001, edited by G. Paschmann and P. W. Daly, pp. 323–348, ISSI/ESA.

Runov, A., V. Angelopoulos, M. I. Sitnov, V. A. Sergeev, J. Bonnell, J. P. McFadden, D. Larson, K.-H. Glassmeier, and U. Auster (2009), THEMIS observations of an earthward-propagating dipolarization front, *Geophys. Res. Lett.*, *36*, L14106, doi:10.1029/2009GL038980.

Runov, A., V. Angelopoulos, X.-Z. Zhou, X.-J. Zhang, S. Li, F. Plaschke, and J. Bonnell (2011), A THEMIS multicase study of dipolarization fronts in the magnetotail plasma sheet, *J. Geophys. Res.*, *116*, A05216, doi:10.1029/2010JA016316.

Runov, A., V. Angelopoulos, C. Gabrielse, X.-Z. Zhou, and D. Turner (2012), Multi-point observations of dipolarization front formation by magnetotail reconnection, *J. Geophys. Res.*, *117*, A05230, doi:10.1029/2011JA017361.

Russell, C. T., M. M. Mellot, E. J. Smith, and J. H. King (1983), Multiple spacecraft observations on interplanetary shocks: Four spacecraft determination of shock normals, *J. Geophys. Res.*, *88*, 4739–4748.

Schmid, D., M. Volwerk, R. Nakamura, W. Baumjohann, and M. Heyn (2011), A statistical and event study of magnetotail dipolarization fronts, *Ann. Geophys.*, *29*(9), 1537–1547, doi:10.5194/angeo-29-1537-2011.

Sergeev, V., V. Angelopoulos, S. Apatenkov, J. Bonnell, R. Ergun, R. Nakamura, J. McFadden, D. Larson, and A. Runov (2009), Kinetic structure of the sharp injection/dipolarization front in the flow-braking region, *Geophys. Res. Lett.*, *36*, L21105, doi:10.1029/2009GL040658.

Sitnov, M. I., M. Swisdak, and A. V. Divin (2009), Dipolarization fronts as a signature of transient reconnection in the magnetotail, *J. Geophys. Res.*, *114*, A04202, doi:10.1029/2008JA013980.

Sonnerup, B. U. Ö., and M. Scheible (1998), Minimum and maximum variance analysis, in *Analysis Methods for Multi-Spacecraft Data, ISSI Scientific Report*, vol. SR-001, edited by G. Paschmann and P. W. Daly, pp. 185–220, Int. Space Sci. Inst. Bern, Switzerland, and Eur. Space Agency, Paris, France.

Vapirev, A. E., G. Lapenta, A. Divin, S. Markidis, P. Henri, M. Goldman, and D. Newman (2013), Formation of a transient front structure near reconnection point in 3-D pic simulations, *J. Geophys. Res. Space Physics*, *118*, 1435–1449, doi:10.1002/jgra.50136.

Woolliscroft, L. J. C., H. S. C. Alleyne, C. M. Dunford, A. Sumner, J. A. Thompson, S. N. Walker, K. H. Yearby, A. Buckley, S. Chapman, and M. P. Gough (1997), The Digital Wave Processing Experiment on Cluster, *Space Sci. Rev.*, *79*, 209–231, doi:10.1023/A:1004914211866.

Zeldovich, Y. B., and Y. P. Raizer (1966), Elements of gasdynamics and the classical theory of shock waves, in *Physics of Shock Waves and High-Temperature Hydrodynamic Phenomena,* chap. 1, edited by W. D. Hayes and R. F. Probstein, Academic Press, New York.